Imaging and Post-Processing of Early Combustion in a Spark-Ignition Engine via Endoscopic Access

S. Shawal, J.B. Saedon, M.S. Meon, N.H. Mohamad Nor*
Faculty of Mechanical Engineering, Universiti Teknologi MARA, 40450 Shah Alam, Selangor, Malaysia
**syahar6595@uitm.edu.com.my*

S. A. Kaiser
IVG, Institute for Combustion and Gas Dynamics- Reactive Fluids, University of Duisburg-Essen, Germany

ABSTRACT

Two different high-speed cameras, a Photron SA-Z and a Vision Research Phantom v7.3, were used together with a large-aperture endoscopic system to visualize the early flame in a nearly unmodified production IC engine. At very low light levels, the patterned read-out noise on the Phantom v7.3 becomes significant. Filtering in the Fourier domain was effective in suppressing this noise component to acceptable levels. A previously-developed algorithm with automatic dynamic thresholding was expanded to separately detect spark ignition and flame kernel in the image sequences. The robustness of the algorithm was examined by processing data sets from different engine operating conditions as well as at different levels of lens collection efficiency (f-number) for the same engine operating point.

Keywords: *Endoscopic imaging; Flame propagation; Spark-ignition engine; Image post-processing; Thresholding*

Introduction

Flame chemiluminescence imaging from excited hydroxyl, OH- and CH radicals [1,2], and sodium- contained fuel additive [3] have been carried out in

ISSN 1823- 5514, eISSN 2550-164X
Received for review: 2019-07-23
Accepted for publication: 2019-10-25
Published: 2020-06-30

spark ignition (SI) engines, mainly to investigate combustion events, in particular with respect to engine cyclic variability.

However, most of these studies were carried out in optical engines with fully optical access. The heavy modifications to the engine limit the engine speed and load and change heat transfer behavior. The large optical access in a research engine, on the other hand, allows low-light imaging through large-aperture lenses with good light-collection efficiency.

The main advantage of endoscopic access is the ability to operate the engine at higher speed and load range as close as possible to that of the metal engine. Chemiluminescence signal from premixed combustion in SI engines is relatively weak, much of it in the UV spectrum range. However, the previous works have shown that the new UV-transparent endoscope [10] has the ability to detect much weaker signals, like those from premixed combustion [11][13] or LIF in the UV [12].

In this paper we evaluate how well the premixed flame front can be detected from broadband CL imaging through such an endoscope system. Fourier-domain filtering is used for images from one of the cameras. In extension of our previous work [13], an improved algorithm was developed to simultaneously extract the shape of the early premixed flame and that of spark.

Experiments

Engine

Experiments were carried out in a 4-cylinder production spark-ignited engine, equipped with an endoscopic system. The engine was operated at stoichiometric condition with engine speed at 2000 rpm and 75 Nm of torque. The engine parameters and operation conditions are tabulated in Table 1.

Table 1: Engine parameters and operating conditions

Engine	BMW N46B20
Compression ratio	10
Displacement per cyl. [cm^3]	499
Bore / stroke [mm]	84 / 90
Speed [min^{-1}] / load [Nm]	2000 / 75
Fuel	Gasoline
IMEP [bar]	4.4

Endoscopic imaging systems

The optical arrangement of the experiments is shown in Figure 1.

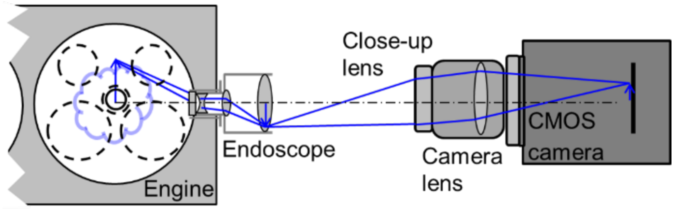

Figure 1: Engine and optics.

The endoscopic system utilizes two stages concept. The endoscope was mounted in the engine to form the first projection image on the lens. The projection creates a Field of View (FOV) with about 40 mm diameter in the center of the engine cylinder. A relay optic, then projected the first image onto the detector sensor. In this experiment, this endoscopic system was coupled with two different camera systems. The characteristics of the cameras are summarized in Table 2.

Table 2: Camera specifications and parameters of the imaging systems. CU = achromatic close-up lens

	Phantom v7.3	Photron SA-Z
Pixel size	22.0 µm^2	20.0 µm^2
Read noise	21e$^-$ rms	29e$^-$ rms
Sensor size	17.6 x 13.2 mm	20.5 x 20.5 mm
Frame rate	6.7 kHz @ 800 x 600 px	20 kHz @ 1024 x 1024 px
Exp. time	20 µs	20 / 12 µs
Rep. rate	11 kHz	20 / 75 kHz
Actual ROI	608 x 456 px	860 x 660 px / 552 x 384 px
Projected pixel size	50 µm/px	35 µm/px
Lens system	50 mm f/1.2 + 250 mm CU	50mm f/1.2 + 250 mm + 500 mm CU

Both cameras are active-pixel CMOS cameras capable of kHz frame rates. However, they are most sensitive in a spectral range between 400 and 800 nm. In premixed flames, such broadband sensing in the visible mainly detects the luminescent species CH*, CO, CO_2, and H_2O. These may not be directly associated with the flame front, but our previous work had shown that nevertheless reasonable information on spark and flame could be extracted from broad-band imaging.

Results and discussion

Wide-field imaging: Variation of camera and aperture

Figure 2a shows samples from the Photron SA-Z at the maximum relay lens aperture f/1.2.

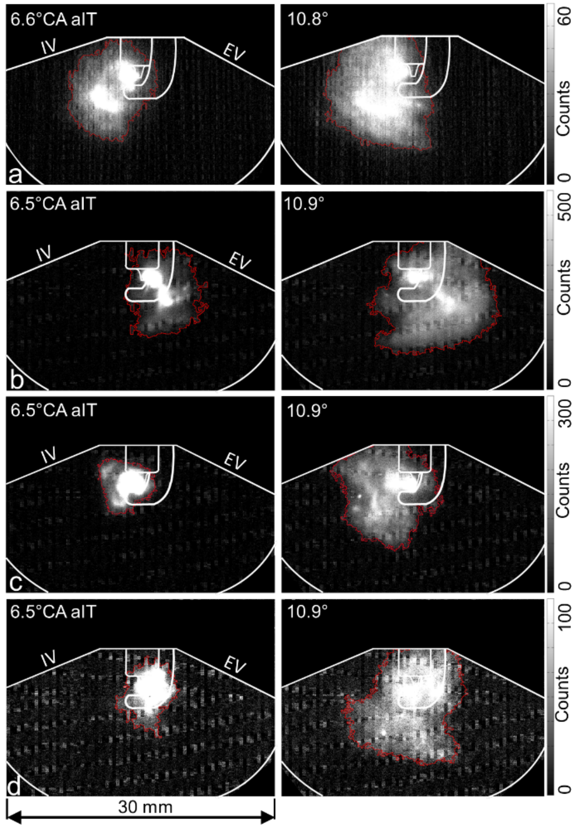

Figure 2: Sample of image series for different imaging system and lens aperture. The red line indicates the flame front as detected by the binarization process. (a) Photron SA-Z, (b-d) Phantom v7.3 with the relay lens at (b) f/1.2, (c) f/2.8, and (d) f/5.6.

Compared to images from the Phantom v7.3 in Figure 2b, the image “quality” appears similar. This is consistent with the specifications listed in Table 2: Read noise is higher, but the sensor area is larger, and at low light levels, both read, and photon noise are relevant. On a per-pixel level, however, the images from the SA-Z had significantly worse signal-to-noise because of the smaller projected pixel size, or equivalently, the higher resolution. For further comparison, the SA-Z images were resized by a factor of 1.5, to 573 x 440 pixels, by interpolation. The projected pixel size is then nearly the same. Of course, the newer Photron SA-Z is much faster than the older Phantom v7.3, which can help analyzing fast phenomena such as the spark, as discussed below. Figure 2b-d shows image samples from the Phantom v7.3 at different apertures[13]. With reduced aperture, signal is lost, but not as much as the reduction in the entrance pupil would indicate. This is due to the fact that the relay lens is imaging off the field lens, which is not an isotropic light source, but directs the rays towards the relay.

The Phantom v7.3 CMOS detector shows a periodic and moving pattern in the read-out noise. To lower the pattern noise, each image was subtracted with the last 10 dark images in each cycle. The image sequence in Figure 2b show that this works quite well for the late crank angles after ignition, because of high signal intensity at this stage of combustion. However, in the early phase of combustion the intensity of flame kernel close to the read out noise. The effect of the periodic noise on images becomes more obvious for datasets at higher f-number (f/2.8 and f5.6) for the same engine operating conditions, as shown in Figure 2c and Figure 2d respectively. Figure 3a shows a close-up of one of the images from the f/5.6-series. In order to reduce the effect of the periodic noise on image, a Fourier filtering technique was applied. Because the noise is patterned, it is associated with distinct regions in the Fourier magnitude image, shown in Figure 3c. These regions can be identified and set to zero. Back-transformation yields significantly lower background level, as seen in Figure 3c. The red line indicates the border of the burnt area, identified by the binarization algorithm described below.

Predictor-corrector binarization scheme

In order to obtain some statistical results, we developed an algorithm that exploits the temporal correlation of the high-speed images in a predictor-corrector scheme, dynamically adjusting the intensity threshold for image segmentation.

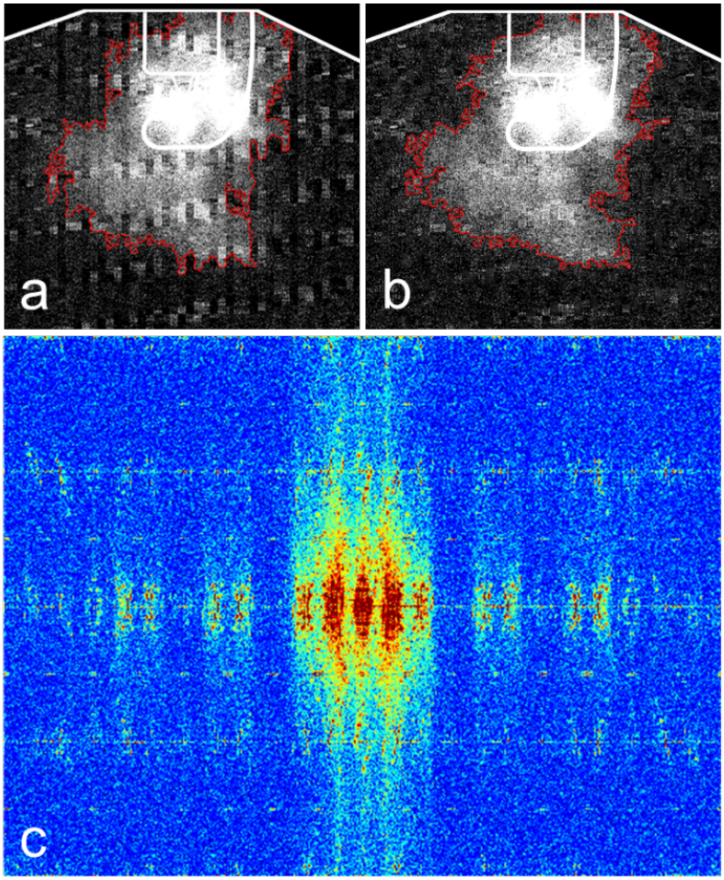

Figure 3: Pattern-noise suppression by Fourier filtering. (a) and (b): Enlarged area of an image from the Phantom v7.3 at a relay lens aperture of f/5.6. (a) after background subtraction, (b) after additional Fourier filtering. (c) Magnitude of the Fourier transform of a dark image, displayed on a logarithmic false-color scale with blue indicating low, red high values.

It is described in [13] and summarized below, including further improvements made since.

1. **Background subtraction**

2. **Fourier filtering via Fast Fourier Transform (FFT)**

3. **Spatial median filtering**

4. Thresholding: Predictor-corrector scheme

In this paper, we propose a new thresholding scheme to segment sequence of flame images into two classes; background and foreground (flame). The main principle of the algorithm is shown in Figure 4. Flame images are used as input to calculate and predict the threshold value of the image based on Otsu's method. The threshold value of the current image is corrected to compute the flame boundary. The main idea is to exploit the images' correlation in time to predict a suitable binarization threshold from the previous image. The algorithm is expected to compute the projected burnt area, which will be used to obtain the flame characteristics in a fast, robust, and reliable way. We summarize the entire process of the algorithm in Figure 5.

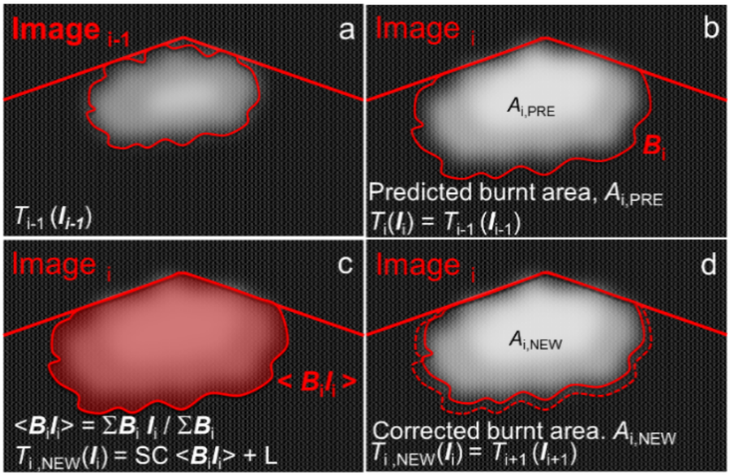

Figure 4: Principle of the predictor-corrector binarization scheme

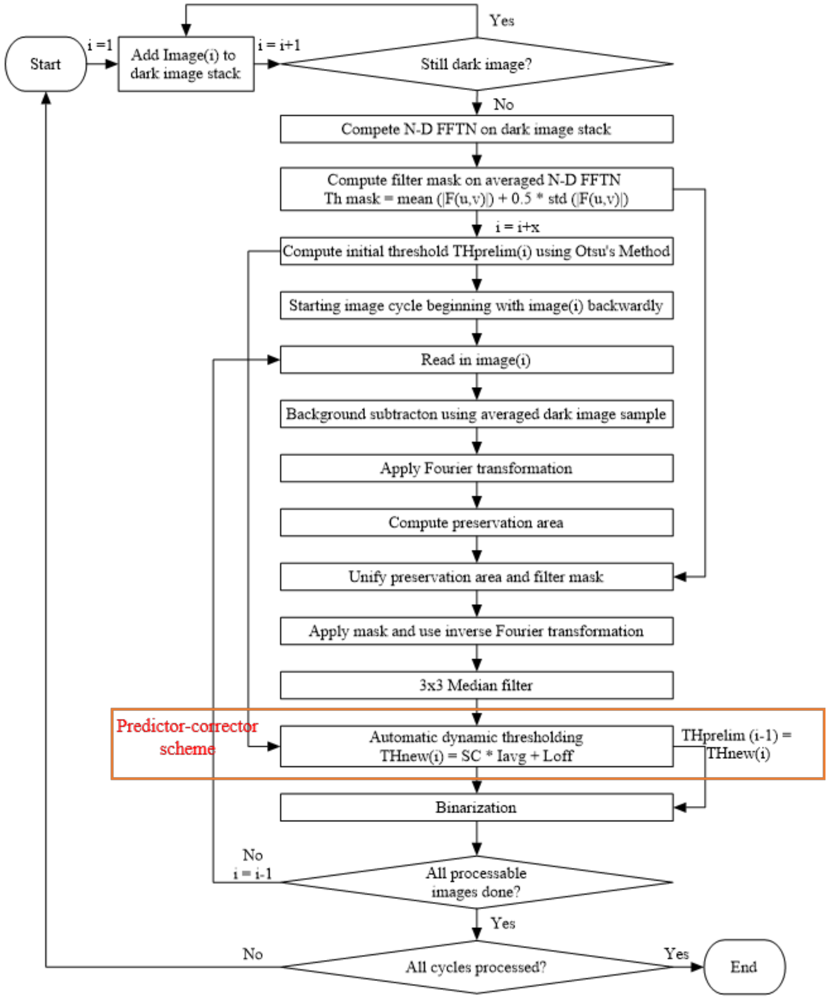

Figure 5: Sketch of the principle of the predictor-corrector binarization scheme.

Equivalent flame radius

In this section, the "quality" of the binarization procedure was examined by plotting the flame radius as a function of time, derived from endoscopic high-speed image sequences.

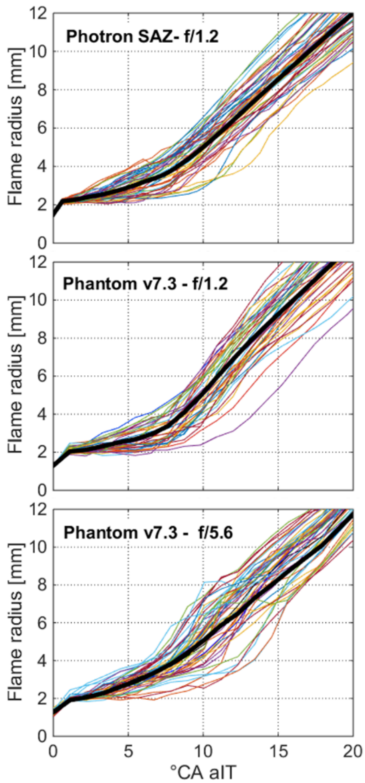

Figure 6: Flame radius for 50 consecutive cycles (colored lines) and the multi-cycle mean of these 50 cycles (solid black line). Camera systems are indicated in each graph.

Figure 6 shows the equivalent flame radius for the two cameras and for the Phantom v7.3 for the largest f-number. Consistent with the visual appearance of the images in Figure 2a and b, the two plots are very similar. There is a small systematic deviation, which may be due slightly different thermal conditions in the engine. In both plots, scatter is low, and lines mostly do not cross, which is physically plausible [1, 2].

For the Phantom v7.3, results from f/2.8 are very similar to those from f/1.2, and (not shown) results without Fourier filtering are also similar. However, at f/5.6, Figure 6c, scatter at early crank angles appears despite Fourier filtering.

Conclusions

Early flame-front propagation was investigated with a large-aperture UV endoscope in a nearly unmodified production SI engine. Two different unintensified high-speed imaging systems with two different CMOS camera were applied and compared in terms of detecting premixed burnt area. The projected burnt area was derived by morphological post-processing. A new edge detection scheme was introduced to enhance the accuracy of early kernel detection. FFT filtering process increases the robustness of the algorithm for detecting the flame boundary at low light conditions.

References

[1] P. G. Aleiferis, A. M. K. P. Taylor, K. Ishii, Y. Urata, "The nature of early flame development in a lean-burn stratified-charge spark-ignition engine", *Combust. Flame,* vol. 136, pp. 283–302, 2004.

[2] P. G. Aleiferis, A. M. K. P. Taylor, J. H. Whitelaw, K. Ishii, Y. Urata, "Cyclic Variations of Initial Flame Kernel Growth in a Honda VTEC-E Lean-Burn Spark-Ignition Engine", *SAE Technical Paper*, 2000-01-1207, 2000.

[3] R. N. Dahms, M. C. Drake, T. D. Fansler, T.-W. Kuo, N. Peters, "Understanding ignition processes in spray-guided gasoline engines using high-speed imaging and the extended spark-ignition model SparkCIMM. Part A: Spark channel processes and the turbulent flame front propagation", *Combust. Flame* 158, pp. 2229–2244, 2011.

[4] V. Salazar, S. A. Kaiser, "Influence of the Flow Field on Flame Propagation in a Hydrogen-Fueled Internal Combustion Engine", *SAE Int. J. Engines,* vol. 4, pp. 2376-2394, 2011.

[5] R. Collin, J. Nygren, M. Richter, M. Aldén, L. Hildingsson, B. Johansson, "Simultaneous OH- and Formaldehyde-LIF Measurements in an HCCI Engine", *SAE Technical Paper*, 2003-01-3218, 2003.

[6] S. H. R. Müller, B. Böhm, M. Gleißner, S. Arndt, A. Dreizler, "Analysis of the temporal flame kernel development in an optically accessible IC engine using high-speed OH-PLIF", *Applied Physics B* 100, pp. 447–452, 2010.

[7] T. Shiozaki, H. Nakajima, Y. Kudo, A. Miyashita, Y. Aoyagi, "The Analysis of Combustion Flame in a Dl Diesel Engine", *SAE Technical Paper*, 960323, 1996.

[8] M. Bakenhus, R. D. Reitz, "Two-Color Combustion Visualization of Single and Split Injections in a Single-Cylinder Heavy-Duty D.I. Diesel Engine Using an Endoscope-Based Imaging System", *SAE Technical Paper*, 1999-01-1112, 1999.

[9] U. Dierksheide, P. Meyer, T. Hovestadt, W. Hentschel, "Endoscopic 2D particle image velocimetry (PIV) flow field measurements in IC engines", *Experiments in Fluids* 33, pp. 794–800, 2002.
[10] R. Reichle, C. Pruss, C. Gessenhardt, C. Schulz, W. Osten, "Diffractive/refractive (hybrid) UV-imaging system for minimally-invasive metrology: Design, performance, and application experiments", *Applied Optics* 511, pp. 982-1996, 2012.
[11] M. Goschütz, C. Schulz, S. A. Kaiser, "Endoscopic imaging of early flame propagation in a near-production engine", *SAE Int. J. Engines* 7, pp. 351-365, 2014.
[12] C. Gessenhardt, C. Schulz, S. A. Kaiser, "Endoscopic temperature imaging in a four-cylinder IC engine via two-color toluene fluorescence", *Proceedings of the Combustion Institute* 35, pp. 3697–3705, 2015.
[13] S. Shawal, M. Goschutz, M. Schild, S. Kaiser, M. Neurohr, J. Pfeil, T. Koch, "High-Speed Imaging of Early Flame Growth in Spark-Ignited Engines Using Different Imaging Systems via Endoscopic and Full Optical Access", *SAE Int. J. Engines* 9, pp. 704-718, 2016.
[14] N. Otsu, "A Threshold Selection Method from Gray-Level Histograms", *IEEE Transactions on systems, Man, and Cybernetics* VOL. SC-9, NO. 1, 1979.